Journal of Magnetic Resonance 212 (2011) 265–273

Contents lists available at ScienceDirect

Journal of Magnetic Resonance

journal homepage: www.elsevier.com/locate/jmr

Multi-quantum echoes in $GdAl_2$ zero-field high-resolution NMR

J.R. Tozoni [a,1], J. Teles [a,2], R. Auccaise [b,3], R. Oliveira-Silva [a], C. Rivera-Ascona [a], E.L.G. Vidoto [a], A.P. Guimarães [b], I.S. Oliveira [b], T.J. Bonagamba [a,*]

[a] Instituto de Física de São Carlos, Universidade de São Paulo, Caixa Postal 369, São Carlos 13560-970, SP, Brazil
[b] Centro Brasileiro de Pesquisas Físicas, Rua Dr. Xavier Sigaud 150, Rio de Janeiro 22290-180, RJ, Brazil

ARTICLE INFO

Article history:
Received 31 May 2011
Revised 4 July 2011
Available online 13 July 2011

Keywords:
High-resolution
Zero-field NMR
Multiple echoes
Intermetallic compounds
Electric quadrupolar coupling
Quadrupolar oscillation

ABSTRACT

In this paper we present a series of high-resolution zero-field NMR spectra of the polycrystalline intermetallic compound $GdAl_2$. The spectra were obtained with the sample at 4.2 K in the ordered magnetic state and in the absence of an external static magnetic field. Using a sequence composed of two RF pulses, we obtained up to five multi-quantum echoes for the ^{27}Al nuclei, which were used to construct the zero-field NMR spectra. The spectra obtained from the FID observed after the second pulse and the even echoes exhibited higher resolution than the odd ones. In order to explain such behavior, we propose a model in which there are two regions inside the sample with different inhomogeneous spectral-line broadenings. Moreover, with the enhanced resolution from the FID signal, we were able to determine quadrupolar couplings with great precision directly from the respective spectra. These results were compared with those obtained from the quadrupolar oscillations of the echo signals, and showed good agreement. Similar data were also obtained from ^{155}Gd and ^{157}Gd nuclei.

1. Introduction

The intermetallic compound $GdAl_2$ has been studied largely by zero field NMR [1–9]. More recent articles have also discussed the conditions for the appearance of its spin glass behavior [10–12]. The compound has the cubic Laves phases structure and the unit cell is formed by sixteen Al atoms forming four tetrahedra with a three-fold symmetry axis along the principal diagonal of the unit cell [1], interspaced with eight Gd atoms in a diamond-like structure. Below 176 K it is in the ferromagnetically ordered state, with the easy magnetization axis along the $\langle 1\,1\,1\rangle$ direction within domains. In each tetrahedron, there are three symmetrically equivalent atoms with respect to the easy magnetization direction. Therefore, for the Al atoms there are two magnetically active sites with a 3:1 ratio, corresponding to the (b,c,d) and a atoms, respectively, in the usual notation [7].

A lot of research has been carried out to determine and explain the zero-field NMR spectra as well as the quadrupolar couplings in this compound. Two main peaks have been reported, which we will label α and β, around 50 MHz and 60 MHz, respectively. Moreover, quadrupolar couplings around 270 kHz for the α peak and 550 kHz for the β peak were also reported. In early reports, those peaks were attributed to the two magnetic sites within domains, since the peak intensities are roughly in the ratio 3:1. However, since in this compound the domain walls are wide and the wall and domain enhancement factors are similar, some authors [5,7,9] have argued that the β peak arises from regions in the domain wall centers on the hard axis of magnetization $\langle 1\,1\,0\rangle$. In particular, Bowden et al. [5] calculated the angular dependencies of the hyperfine field and the quadrupolar couplings for each site of the ^{27}Al atoms and showed that the a atoms within domains contribute mainly to the α peak, while the c and d atoms in domain walls contribute to the β peak. This interpretation was further reinforced by Dumelow et al. [7] with new NMR measurements, including the application of an external magnetic field to powdered and single-crystal samples. Bauer and Dormann [9], based on high-field single-crystal NMR data, extrapolated the NMR frequencies to the zero-field case and to different radio frequency (RF) amplitudes. Their results, as well spectrum simulations, suggested that only the domain wall centers and edges contribute to the whole ^{27}Al NMR spectrum.

As an alternative approach to finding the quadrupolar couplings, many authors have utilized the quadrupolar oscillation method of the echo amplitude, described by Abe et al. [13]. It has been found that better resolution spectra are obtained from single-crystal samples or polycrystalline samples that are not finely powdered. For example, Dumelow et al. [7] utilized the central line of the quadrupolar quintuplet to obtain precise values of the

* Corresponding author.
E-mail address: tito@ifsc.usp.br (T.J. Bonagamba).
[1] Present address: Instituto de Física, Universidade Federal de Uberlândia, Caixa Postal 593, Uberlândia 38400-144, MG, Brazil.
[2] Present address: Centro de Ciências Agrárias, Universidade Federal de São Carlos, Araras 13600-970, SP, Brazil.
[3] Present address: Embrapa Solos, Rio de Janeiro 22460-000, RJ, Brazil.

1090-7807/$ - see front matter © 2011 Elsevier Inc. All rights reserved.
doi:10.1016/j.jmr.2011.07.003

hyperfine field. In this paper we also present well-resolved spectra for a powder $GdAl_2$ sample. Besides the enhanced spectral resolution, we were able to record the FID signal and all five multi-quantum (MQ) echoes expected for the ^{27}Al nuclei (spin 5/2), due to the quadrupolar interaction, using a two pulse sequence. To our knowledge, this has never been reported before for this compound. The access to high-resolution MQ-echo spectra opens up new possibilities of analysis of the hyperfine field and quadrupolar coupling distributions for magnetic samples.

The paper is organized as follows. Section 2 presents the simplified Hamiltonian which describes the main features of the NMR signals in the $GdAl_2$ sample. Section 3 presents a brief review of the dependence of the MQ-echo spectra line widths on the hyperfine field and quadrupolar coupling distributions. Experimental results are presented in Section 4. At first, we present the ^{155}Gd and ^{157}Gd spectra obtained from the FID and the MQ-echo signals. Next, we present the ^{27}Al spectrum derived from the FID signal produced by a single pulse sequence, where the dead time between excitation and signal acquisition, ~2 μs, was shorter than the transverse relaxation time (T_2), ~25 μs. Then, using a sequence of two identical RF pulses, we varied the pulse lengths in order to maximize the amplitude of the five MQ echoes for the ^{27}Al signal. From the corresponding spectra, we found that the even echoes (2,4) presented narrower line widths than the odd ones (1,3,5). Additionally, the well-resolved quadrupolar couplings obtained from the spectra were compared with those obtained by the quadrupolar oscillation method, showing good agreement. In Section 5, we discuss the experimental results based on the expected line widths calculated in Section 3, which lead us to conclude that the NMR signal from the ^{27}Al nuclei originate from two distinct hyperfine field distributions. Conclusions are drawn in Section 6.

2. Origin of the NMR signal

The nuclear Hamiltonian for both quadrupolar nuclei at the nth site in the $GdAl_2$ can be separated into three parts: [9]

$$H_n = H_{eff,n} + H_{q,n} + H_{rf,n}. \tag{1}$$

The effective Hamiltonian H_{eff} can be approximated by the Zeeman interaction with the effective magnetic field:

$$\vec{B}_{eff,n} = \vec{B}_{hf,n} + \vec{B}_{d,n} + \frac{4}{3}\pi\vec{M}_s, \tag{2}$$

where $\vec{B}_{hf}$ accounts for the interaction with the polarized conduction electrons, $\vec{B}_d$ is the dipolar field due to the Gd^{3+} electron momenta, and $\frac{4}{3}\pi\vec{M}_s$ is the Lorentz field. Since H_{eff} is the principal contribution to H, for each site n we define a frame with the z-axis parallel to $\vec{B}_{eff,n}$. Assuming cylindrical symmetry for the electric field gradient (efg) at the nuclei sites, the quadrupolar interaction, to first-order approximation, is given by:

$$H_{q,n} = \hbar\frac{\omega_{q,n}}{6}\left[3I_z^2 - I(I+1)1\right], \tag{3}$$

where I_z is the component of the nuclear angular momentum operator along the z direction of site n, I is the nuclear spin quantum number, and $\omega_{q,n}$ the quadrupolar coupling amplitude.

The RF Hamiltonian H_{rf} corresponds to the interaction of the nuclei with the applied RF field $\vec{B}_{rf}$. Since it is a perturbative term of H_{eff}, only the components perpendicular to the z-direction in the nth frame need be considered:

$$\vec{B}_{rf,n}(t) = B_{rf,n}[\cos(\omega t + \phi_n)\hat{x} + \sin(\omega t + \phi_n)\hat{y}]. \tag{4}$$

The system dynamics is more easily described in a rotating frame around the z-direction of each site with the RF field angular frequency ω, giving the transformed Hamiltonian:

$$\widetilde{H}_n = -\hbar(\omega_{0,n} - \omega)I_z + \hbar\frac{\omega_{q,n}}{2}I_z^2 - \hbar\omega_{1,n}I_{\phi,n}. \tag{5}$$

The new amplitude variables are defined by $\omega_{0,n} = \gamma B_{eff,n}$ and $\omega_{1,n} = \gamma B_{rf,n}$, where γ is the nuclear gyromagnetic ratio. $I_{\phi,n}$ is the component of the angular momentum perpendicular to the z-axis and making an angle ϕ,n with the x axis of the nth frame.

We can see that the dependence on n of all the interactions above are due to two causes: (i) variation, from site to site, of the interaction amplitudes and (ii) variation of the relative orientations of $\vec{B}_{eff,n}$ with respect to the efg symmetry axis and $\vec{B}_{rf,n}$.

In order to describe the density matrix evolution of the system we can substitute the dependence on the discrete variable n by that on a continuous distribution:

$$p(\omega_0, \omega_q, \omega_1) = f(\omega_0)g(\omega_q)h(\omega_1), \tag{6}$$

where $p(\omega_0,\omega_q,\omega_1)d\omega_0 d\omega_q d\omega_1$ gives the probability of finding a nucleus with interaction amplitudes between ω_0 and $\omega_0 + d\omega_0$, ω_q and $\omega_q + d\omega_q$, and ω_1 and $\omega_1 + d\omega_1$. In fact, ω_1 is a bi-dimensional variable since it also includes the ϕ RF phase dependence. Here we are not interested in describing the exact form of the p distribution, but just in relating its dispersion to the spectral line widths of the NMR echo signals. Therefore, the assumption of uncorrelated distributions expressed in Eq. (6), though not generally true, simplifies the treatment and is sufficient for our purposes. Moreover, if there is no correlation between the amplitude of the $\vec{B}_{eff}$ field and its direction relative to a fixed laboratory frame, the NMR signal is proportional to the usual projection of ρ onto the transverse angular momentum operator:

$$S(t) = Tr\{I_+ \int \rho(\vec{\omega}, t)p(\vec{\omega})d\vec{\omega}\}, \tag{7}$$

where $\rho(\vec{\omega}, t)$ is the solution of the Liouville-von Neumann equation for the Hamiltonian of Eq. (5) and $I_+ = I_x + iI_y$. The symbol $\vec{\omega}$ is just a compact notation for $(\omega_0,\omega_q,\omega_1)$. Here we assume that the true relaxation times are much longer than the inverse of the interaction amplitudes dispersion.

3. General properties of the MQ echoes

Almost all NMR interactions can give rise to MQ states, including the dipole and quadrupolar interactions in solids and the J coupling in liquids. A way to reveal such states is to observe the formation of multiple echoes for quadrupolar nuclei in the presence of spatial distributions of the interaction amplitudes through the sample. Hahn was the first to explore the NMR echo phenomenon due to the static magnetic field inhomogeneity [14]. Solomon described the MQ echoes due to the quadrupolar coupling inhomogeneity in solid crystals [15]. Since then, many works have described MQ echo formation in a great variety of materials and interaction strengths and distributions [16–25]. Echo formation is especially important in the study of magnetic materials, since the great interaction dispersion can let the FID signal vanish before the start of acquisition. Moreover, valuable information about the nature of the MQ states can be extracted from the spectra of the echoes. We will focus only on the contribution of the quadrupolar interaction to the MQ states generation. The inhomogeneity of the quadrupolar and the Zeeman interactions will be responsible for the spectral line shape structure in the multiple echo signal. Only the half-integer spin will be treated, since this is the case for both the Gd and Al nuclei. It is worth mentioning that, besides the quadrupolar interaction, there are at least two other mechanisms for the formation of multiple echoes: dynamic effects due to hyperfine magnetic interactions [24] and stimulated echoes [14] due to short repetition times compared with the relaxation times. We neglect the former, owing to the absence of

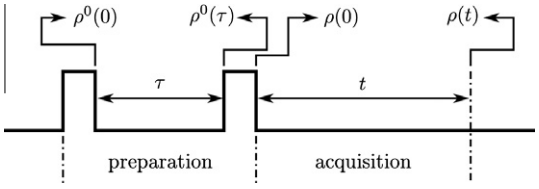

Fig. 1. Pulse sequence for MQ states and echo generation. The two RF pulse widths are much shorter than τ.

experimental evidence for the compound $GdAl_2$, while the latter can be suppressed by using sufficiently long repetition times.

Here we consider the two-pulse sequence shown in Fig. 1. To facilitate the analysis we assume that there are no Zeeman and quadrupolar interaction dispersions during the application of the RF pulses, that is, Hamiltonian (5) is independent of the n sites. This assumption, together with condition (6), enables us to relate the MQ echo shapes directly to the Fourier transforms (FT) of distributions $f(\omega_0)$ and $g(\omega_q)$. Moreover, since the pulse widths are much shorter than the evolution period, τ, echoes are predominantly dictated by the distributions f and g in the intervals where there are no RF fields.

Starting from the thermal equilibrium state of zero-order coherence, in the presence of the quadrupolar interaction, the first pulse will create a state of multiple quantum coherences ρ^0. During the evolution period, τ, each matrix element ρ^0_{ij} will gain a phase proportional to the Bohr frequency v_{ij} of Hamiltonian (5) without the RF term: $\rho^0_{ij}(\tau) = \rho^0_{ij} e^{iv_{ij}\tau}$. The second pulse will mix the different $\rho^0_{ij}(\tau)$ terms, and the new elements will be related to the old ones by the transformation $\rho_{kl}(0) = \sum_{ij} a^{kl}_{ij} \rho^0_{ij}(\tau)$. The transformation elements are given by $a^{kl}_{ij} = U_{ki} U^{-1}_{jl}$, where U is the propagator for the second pulse. For $t > 0$, the coherence phases will evolve again and the matrix elements will be given by $\rho_{kl}(t) = \sum_{ij} a^{kl}_{ij} \rho^0_{ij} e^{i\theta^{kl}_{ij}(t)}$, where $\theta^{kl}_{ij}(t) = v_{ij}\tau + v_{kl}t$. Echoes will occur at times when the phases θ^{kl}_{ij} are independent of the amplitudes ω_0 or ω_q. Substituting $\rho(t)$ in Eq. (7) we obtain the following expression for the NMR signal:

$$S(t) = \sum_{ijk} c^k_{ij} F(t - \xi_{ij}) G(\chi_{ij} - \alpha_k t) e^{i\langle v_{k,k-1}\rangle t}, \tag{8}$$

where

$$\xi_{ij} = \tau(m_i - m_j), \tag{9}$$

$$\chi_{ij} = \frac{\tau}{2}\left(m_i^2 - m_j^2\right), \tag{10}$$

$$\alpha_k = m_k + \frac{1}{2}, \tag{11}$$

$$\text{and } \langle v_{k,k-1}\rangle = \langle \omega_q \rangle \alpha_k - \langle \omega_0 \rangle. \tag{12}$$

The coefficients are given by:

$$c^k_{ij} = a^{k,k-1}_{ij} \rho^0_{ij} e^{i\langle v_{ij}\rangle \tau} [I_+]_{k-1,k}. \tag{13}$$

The summation indexes cover the range $-I \leqslant m_i,\ m_j \leqslant I$ and $-I \leqslant m_k < I$, where the variables m correspond to magnetic quantum numbers. The functions F and G are the Fourier transforms of the distributions $f(\langle\omega_0\rangle + \omega_0)$ and $g(\langle\omega_q\rangle + \omega_q)$, where we will assume that f and g are real functions symmetrical around the mean values $\langle\omega_0\rangle$ and $\langle\omega_q\rangle$, respectively. Therefore, $F(t')$ and $G(t')$ are real functions, symmetrical around $t' = 0$.

We will define the *echo order* as the time t that corresponds to the center of the functions F and G in units of τ. Thus, $F(t - \xi_{ij})$ and $G(\chi_{ij} - \alpha_k t)$ correspond to echoes of order ξ_{ij}/τ and $\chi_{ij}/\alpha_k\tau$, respectively. From the arguments of the functions we see that the instants of the echo centers are related to the quantum numbers m_i and m_j for function F and m_i, m_j, and m_k for function G. Eq. (13) shows that those echoes will exist only if the first pulse creates the corresponding ρ^0_{ij} coherences and if the second pulse connects those coherences with the first order states $m_k - m_{k-1}$ through the transformation elements $a^{k,k-1}_{ij}$. These elements are obtained from the propagator for the second pulse, taking $\langle\omega_0\rangle$, $\langle\omega_q\rangle$, and $\langle\omega_1\rangle$ as the interaction amplitudes.

The quantum number m_k labels the $2I - 1$ spectral components of frequencies $\langle v_{k,k-1}\rangle$, which are symmetrically distributed around $-\langle\omega_0\rangle$ and equally spaced by $\langle\omega_q\rangle$, as can be shown by Eqs. (11) and (12). Hereafter we will refer to the transitions $m_k \leftrightarrow m_{k-1}$ simply as m_k.

Let $\Delta\omega_0$ and $\Delta\omega_q$ be some measure of the Zeeman and quadrupolar distribution widths, as for example their half widths at half maximum. Three interaction inhomogeneity conditions will be considered separately.

3.1. The Zeeman inhomogeneity case

The Zeeman inhomogeneity case is characterized by the condition:

$$\Delta\omega_q \ll 1/\tau \ll \Delta\omega_0. \tag{14}$$

In this case, we can neglect the effect of the function G in each term of the summation (8), since its temporal width will be much greater than the separation between its center and that of function F. Moreover, for fast-decaying functions, the condition $1/\tau \ll \Delta\omega_0$ implies that the superposition of functions F with different arguments ξ_{ij} can be neglected. Therefore, the echo centers are determined by the times that cancel out the argument in F:

$$t = \tau(m_i - m_j). \tag{15}$$

It follows that an echo of order p will be affected only by the coherences ρ^0_{ij} of the same order p created by the first pulse, where the *coherence order* of a density matrix element ρ_{ij} is defined as $m_i - m_j$. All the distinct echo centers are equally spaced by τ, and there are at most $2I$ echo orders, besides the zeroth one ($m_i = m_j$) that corresponds to the FID signal of the second pulse.

All $2I - 1$ spectral lines labeled by m_k are expected for any echo and they all have the same line width $\Delta\omega_0$. This can be seen from the argument of the F function, which is independent of m_k.

3.2. The quadrupolar inhomogeneity case

The criterion here is precisely the opposite of that for the previous case:

$$\Delta\omega_0 \ll 1/\tau \ll \Delta\omega_q. \tag{16}$$

In this case, the function F can be neglected in Eq. (8) and the superposition of the various functions G is negligible, in view of the condition $1/\tau \ll \Delta\omega_q$. Thus, the quadrupolar echoes are centered at times that cancel out the argument in G:

$$t = \tau \frac{m_i^2 - m_j^2}{2m_k + 1}. \tag{17}$$

Now, there is no simple relation between the coherence orders of ρ^0 and the echo orders. Many coherences contribute to the same echo and various echoes share the same coherences. For example, the coherences ($m_i = 3/2, m_j = 1/2$) and ($m_i = 3/2, m_j = -1/2$) contribute to the same spectral component $m_k = 1/2$ of the echo centered at $t = \tau$. Moreover, the echoes are not evenly spaced, occurring at intervals of some integer and half-integer multiples of τ, e.g., $t = \tau/2$, τ, $3\tau/2$, 2τ, and 3τ, for $I = 5/2$.

The argument of function G also shows that the time t is scaled by α_k. This implies that the widths of spectral components of a given echo are equal to $\Delta\omega_q|m_k + 1/2|$. Therefore, the line widths of the satellites will be proportional to their distances from the

Table 1
Properties of the MQ echoes for the three inhomogeneity conditions.

Inhomogeneity case	Distributions widths	Echo centers (τ units)	Echo/coherence order relation	Spectral widths
Zeeman	$\Delta\omega_q \ll 1/\tau \ll \Delta\omega_0$	Integers	Biunique	Central: $\Delta\omega_0$ Satellites: $\Delta\omega_0$
Quadrupolar	$\Delta\omega_0 \ll 1/\tau \ll \Delta\omega_q$	Integers and half integers	Non-unique	Central: $\Delta\omega_0$ Satellites: $\Delta\omega_q\lvert m_k + 1/2\rvert$
Complete	$\Delta\omega_0, \Delta\omega_q \gg 1/\tau$	Odd integers	Biunique	Central: $\Delta\omega_0$ Satellites: $\Delta\omega_0 + \Delta\omega_q\lvert m_k + 1/2\rvert$

spectrum center at $-\langle\omega_0\rangle$. Another consequence of the dependence of G on m_k is that not all the $2I-1$ spectral lines will be present in a given echo. For example, for the echo centered at $3\tau/2$, besides the central line, only the extreme satellites $m_k = -5/2$ and $m_k = 3/2$ will contribute to the spectrum of an $I = 5/2$ nucleus.

The spectral analysis of the central line $m_k = -1/2$ deserves special attention, since the denominator of Eq. (17) is zero in this case. Eq. (8) shows that the G function argument is zero at any time for $m_k = -1/2$ and $m_i = \pm m_j$. Therefore, the central line is dictated by the F functions centered at the corresponding ξ_{ij} times. If the condition $\Delta\omega_0 \ll 1/\tau$ is easily satisfied, the FID and all echoes will have a narrow central line of width $\Delta\omega_0$. Otherwise, the farther from $t = \xi_{ij}$ an echo is formed, the more damped will be its central line amplitude.

3.3. The complete inhomogeneity case

The complete inhomogeneity case is characterized by the condition:

$$\Delta\omega_0, \Delta\omega_q \gg 1/\tau. \tag{18}$$

In this case, neither the Zeeman nor the quadrupolar distributions can be neglected. To each term in the summation (8), the functions F and G will cancel each other except when their centers coincide. Therefore, equating the times in Eqs. (15) and (17) and setting the coherence order $p = m_i - m_j$, we find that m_k must satisfy the following equations simultaneously:

$$m_k = m_i - \frac{p}{2} - \frac{1}{2} \tag{19}$$

$$\text{and } m_k = m_j + \frac{p}{2} - \frac{1}{2}. \tag{20}$$

For a fixed p, Eq. (19) gives the upper bound for m_k when $m_i = I$ and Eq. (20) gives the lower bound for m_k when $m_j = -I$:

$$-I + \frac{p}{2} \leqslant m_k + \frac{1}{2} \leqslant I - \frac{p}{2}. \tag{21}$$

It can be seen from Eqs. (19) and (20) that only odd values of p result in valid m_i, m_j, and m_k values. Moreover, condition (21) guarantees that for every odd p there will exist at least one m_k that satisfies Eqs. (19) and (20). Therefore, by Eq. (15), the echoes will be centered at times:

$$t = p\tau, \quad \forall \text{ odd } p. \tag{22}$$

Condition (21) implies that, for each order p echo, only the first $I - p/2$ satellite spectral line pairs will exist. In particular, the spectra of the first order and $2I$th order echoes will feature all the satellites and no satellites at all, respectively.

The central line $m_k = -1/2$ must again be analyzed with the aid of Eq. (8), which tells us that the argument of function G is canceled out for $m_i = \pm m_j$. The minus and plus signs imply odd p and $p = 0$, respectively. Consequently, all echoes and the FID spectra will have a central line width of $\Delta\omega_0$. The satellite widths will be $\Delta\omega_0 + \Delta\omega_q|m_k + 1/2|$, as they contain contributions from both F and G.

Table 1 contains a resume of the three interaction inhomogeneity conditions. Dispersion of either the Zeeman or quadrupolar interactions can produce MQ echoes. In any case, the existence of a strong Zeeman dispersion, $\Delta\omega_0 \gg 1/\tau$, will create a one-to-one relation between the echo and the coherence orders, while only odd orders will exist if a strong quadrupolar dispersion, $\Delta\omega_q \gg 1/\tau$, is also present. There is no simple echo/coherence order relation if only a strong quadrupolar dispersion, $\Delta\omega_0 \ll 1/\tau \ll \Delta\omega_q$, is present. Finally, only the Zeeman inhomogeneity case will produce all $2I$ spectral lines for all echoes.

4. Experimental results

The $GdAl_2$ compound was prepared by the voltaic arc technique under an argon atmosphere, followed by thermal treatment [26]. Subsequently, the specimen was milled into a powder. The powder was analyzed by X-ray diffraction and the XRD pattern compared to that of $GdAl_2$ in the database at JCPDS-International Centre for Diffraction Data [Id Number 28-0021, PCPDFWIN Version 2.1, 2000]. For the measurements, the powdered sample (~100 mg) was mixed with mineral oil. The grain sizes were estimated to be from 1 to 10 μm by optical microscopy.

The ^{155}Gd, ^{157}Gd, and ^{27}Al zero-field NMR experiments were carried out at 4.2 K with a Discovery Tecmag Console, operated in the frequency range of 1 to 600 MHz. For these wide line experiments, no filtering or tuned elements (including quarter wavelength cables) were used, in order to avoid introducing spectral artifacts.

Since the effective field distribution in ferromagnetic materials is usually very wide, generating NMR spectra much broader then the spectral width of the RF excitation pulse, it is often necessary to perform a pulse frequency sweep [27]. The signals thus obtained were processed by two methods. The first consists in taking, for each frequency step, the modulus of the integral of the real and imaginary parts of the time signal [28]. The second corresponds to the summation of the Fourier transform of the time signal for each frequency step [29].

4.1. Gadolinium spectra

In Fig. 2, we present the NMR time signals and respective spectra for the ^{155}Gd and ^{157}Gd nuclei (14.7% and 15.7% natural abundance, respectively). Both nuclei possess spin 3/2 and thus can present MQ echoes due to quadrupolar interaction. Although the field dispersions are usually wide when compared with non-magnetic materials, for our sample it was small enough to observe the Gd nuclei FID signals. To do that, the two-pulse sequence shown in Fig. 1 was used. The echo time τ was 40 μs and the pulse widths were 1.0 μs for the first and 0.5 μs for the second RF pulse. The RF pulse phases were equal. The repetition time was 100 ms and number of scans 30,720. Figs. 2b and c show the Gd spectra obtained from the Fourier transform of the FID and first and third echoes. It can be seen that only the third echo spectrum does not exhibit the two satellites expected for a $I = 3/2$ nucleus. By estimating the half-line widths at half-maximum of the FID and first echo,

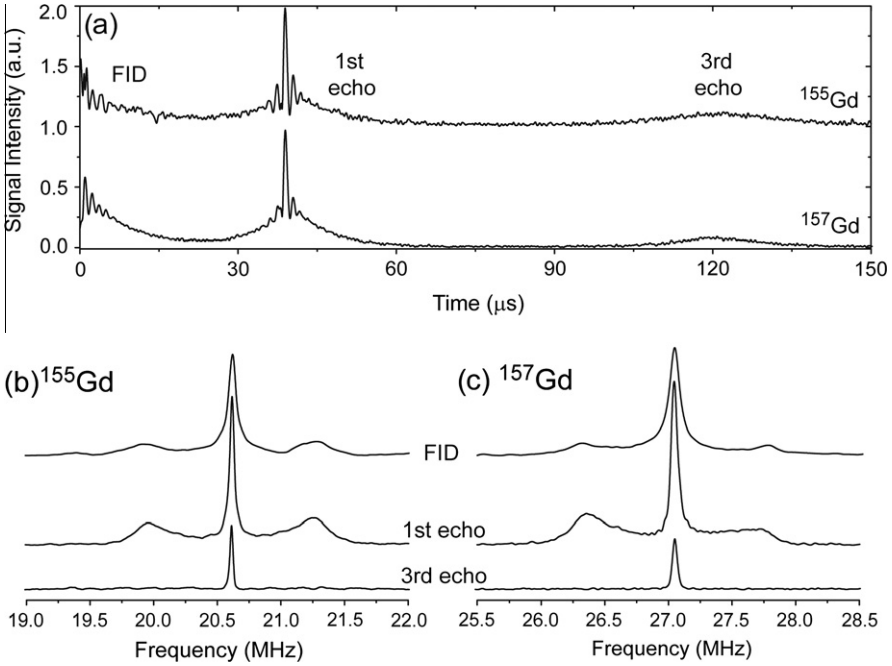

Fig. 2. (a) ^{155}Gd and ^{157}Gd NMR time signal modulus obtained after the two-pulse sequence (Fig. 1). (b) ^{155}Gd and (c) ^{157}Gd spectra obtained from the Fourier transform of the FID and each individual echo shown in (a). The RF pulses were applied at the single carrier frequencies of 20.6 MHz and 27.1 MHz for the ^{155}Gd and ^{157}Gd nuclei, respectively.

we found that the central line is ~50 kHz wide, while the satellites are ~200 kHz wide. According to the theory expounded in Section 3 and summarized in Table 1, those widths enable an estimate of the interaction distributions of $\Delta\omega_0 = 50$ kHz and $\Delta\omega_q = 150$ kHz to be made. It follows that the condition $\Delta\omega_0, \Delta\omega_q \gg 1/\tau(\text{in Hz})$ is satisfied, which characterizes the complete inhomogeneity case for both Gd nuclei. Thus, the complete inhomogeneity condition explains the absence of satellites in the third echo spectrum, since, according to the theory presented in Section 3.3, the highest order echo shows no satellites at all. Fig. 2a shows the Gd nuclei time signals after the two-pulse RF sequence for the echo time $\tau = 40$ μs, from which the spectra of Fig. 2a were obtained. We can easily recognize the FID, the first and the third echoes at $t = 0$ μs, $t = 40$ μs, and $t = 120$ μs, respectively. There is no second order echo at $t = 80$ μs, or its amplitude is negligible, which is again in accordance with the complete inhomogeneity condition discussed in Section 3.3.

The measured quadrupolar couplings from the spectra were ~620 kHz for ^{155}Gd and ~680 kHz for ^{157}Gd. These results are in agreement with the literature for a single-crystalline sample [6], and indicate that the zero-field NMR spectra are independent of crystal orientation [7], since our sample was polycrystalline. We also performed quadrupolar oscillation experiments in order to compare the quadrupolar couplings. However, the results showed no oscillations at all, indicating that this method apparently could not be applied to the Gd nuclei in our sample, thus reinforcing the importance of the high resolution spectra obtained.

4.2. ^{27}Al single pulse spectrum

The magnetic field dispersion at the ^{27}Al sites was also small enough to observe the FID signal after a single pulse excitation. Fig. 3 presents the ^{27}Al FID signal and the corresponding spectrum for the single-pulse sequence. The pulse width was 0.5 μs and the frequency sweep was made in 360 frequency steps covering a bandwidth of 28 MHz, 1,536 scans being taken for each step. The repetition time was 100 ms. The measured quadrupolar couplings

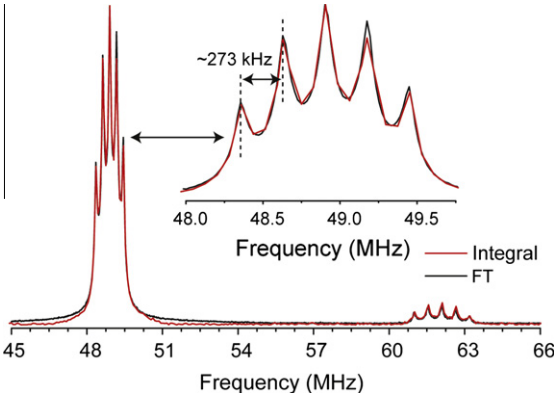

Fig. 3. ^{27}Al NMR spectra of the FID signal generated by the single-pulse sequence. The spectra were collected by pulse frequency sweep and processed by both Integral and FT methods.

were ~270 kHz for the 48.9 MHz peak and ~550 kHz for the 62.1 MHz peak. It can be observed that the quadrupolar lines are well resolved and that second order quadrupolar effects are negligible, since the spectral lines are evenly spaced. These results are consistent with those reported in the literature for the echo signal [3,7]. By fitting a Lorentzian line shape to the spectrum of Fig. 3, we found an average line width of $\Delta\omega \sim 80$ kHz for spectral lines around the 48.9 MHz peak and $\Delta\omega \sim 100$ kHz around the 62.1 MHz peak, where $\Delta\omega$ is the half-width at half-maximum of the Lorentzian distribution. According to Table 1, the approximately equal line widths are indicative of the Zeeman inhomogeneity case or the complete inhomogeneity case with $\Delta\omega_0 \gg \Delta\omega_q$. The line widths were obtained by the Fourier transform method (red line) since this method resulted in a better resolved spectrum.

It is important to mention that the individual multiplet spectra centered at 48.9 and 62.1 MHz could be obtained with the single pulse sequence without a sweeping frequency, provided the pulse bandwidth is broader than 2 MHz (pulse width $\leqslant 0.5$ μs), as is the case here.

4.3. ^{27}Al quadrupolar oscillation of multi-quantum echoes

Here we describe the experimental results for the quadrupolar couplings of the ^{27}Al nucleus, obtained by the quadrupolar oscillation method. Abe et al. [13] deduced that, for the Zeeman inhomogeneity condition, the echo amplitudes oscillate as a function of the echo time τ at frequencies that are multiples of $\langle\omega_q\rangle$. More specifically, the first, second, and third echoes shows harmonic components, multiples of $n\langle\omega_q\rangle$, $(2n+1)\langle\omega_q\rangle$, and $3n\langle\omega_q\rangle$, respectively, where n is a positive integer, including $n=0$ just for the odd echoes. Fig. 4 presents the results for the three first echoes at the frequencies of 48.9 and 62.1 MHz. The amplitudes were measured at the corresponding echo centers, as functions of τ, and then Fourier transformed to give the spectral composition. Odd echoes presented a zero frequency term, as expected, which was subtracted before the transform. It can be seen clearly that the echoes exhibit harmonic components at the expected multiples. Those multiples are consistent with the values of 270 and 550 kHz obtained in Sections 4.2 and 4.4 for the quadrupolar couplings at frequencies 48.9 and 62.1 MHz, respectively. Here, we observe a splitting in the peak structure of echoes 1 and 2 at 62.1 MHz, which is indicative of the presence of two different quadrupolar couplings. This effect is also observed in the first echo spectrum of Section 4.4.

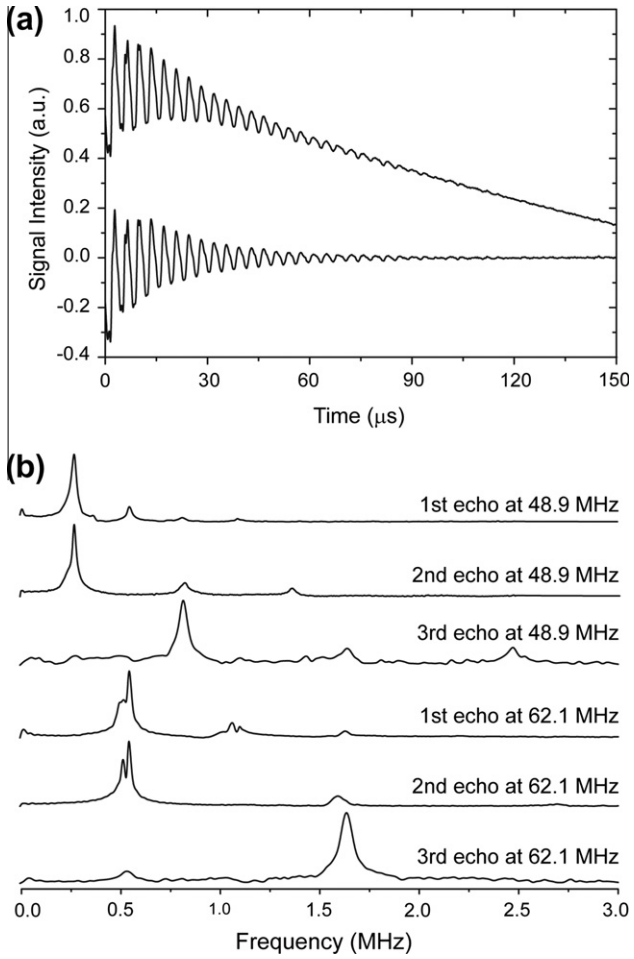

Fig. 4. Raw (top) and baseline-removed (bottom) ^{27}Al quadrupolar oscillation observed for the first echo at 48.9 MHz. (b) Spectral compositions obtained by Fourier transform of the ^{27}Al quadrupolar oscillations measured for the first three echo amplitudes at both 48.9 and 62.1 MHz.

4.4. ^{27}Al FID, multi-quantum echoes and spectra

Here we analyze the FID and all five echoes produced by the ^{27}Al nuclei under the two-pulse sequence. They were obtained at 48.9 MHz, by using first and second pulse widths of 1.2 μs and 0.7 μs separated by a τ interval of 40 μs, a repetition time of 100 ms and 102,400 scans. Fig. 5a shows the FID and all five echo time-domain signals. Fig. 5b–g show the spectra obtained directly by Fourier transform of the FID and echoes, without frequency sweep. The FID spectrum was obtained with time window of 20 μs. The echo spectra were obtained with a rectangular time window of 40 μs, centered at the respective echo centers.

Since the NMR spectrometer was used to detect very wide spectra, special care was taken to avoid spurious artifacts affecting the wide line spectral shape, arising from transmitter, receiver, cables, radio frequency (RF) probe, etc. [30]. In order to circumvent such undesirable contributions, the radio frequency probe coil was designed to avoid self-resonances in the experimental frequency range (10–100 MHz) and its connections to the spectrometer were made without using any tuning/matching by capacitors or transmitter/receiver duplexing with quarter-wavelength-cable. Before the experiments, the following calibration procedures were carried out: (i) the RF probe was fully characterized by the use of a vector impedance meter; (ii) the spectrometer frequency response, without probe, was analyzed by connecting the transmitter directly to the receiver and running the experiment over the full experimental frequency range; and (iii) the procedure used in (ii) was repeated with the inclusion of the RF probe (loop-back experiment). After these procedures, it was possible to observe all the spurious contributions of the spectrometer to the spectra, allowing them to be eliminated safely from the observed spectra. Fig. 6 shows the raw spectrum observed for the first echo together with the loop-back curve and its second derivative, needed to indicate where one can easily observe the spurious artifacts introduced by all the components of the spectrometer. The second derivative is important for this analysis because it indicates that some spurious oscillations found in the spectra are not associated with quadrupolar multiplets, since they do not show the expected multiplet patterns and the quadrupolar oscillation experiments indicate that the splittings are different from that observed. In this way, all the oscillations not correctly correlated with the measured quadrupolar couplings could be removed from the spectra. A splitting of the quadrupolar multiplet structure is seen around the 62.1 MHz; this was also observed in the echo oscillation experiments of Section 4.3, thus indicating that two quadrupolar couplings are really present in this portion of the spectrum, and are not due to some processing artifact.

Fig. 7 shows the spectra obtained from the FID and the first three echoes, employing the same procedures discussed above, and processed by the Fourier Transform method, with the same frequency sweep and average values as in Section 4.2. The pulse widths were 1.2 μs for both the first and second RF pulses. The echo time was $\tau = 70$ μs, the repetition time 100 ms, and 2048 scans were taken. The three echoes were equally spaced by the interval τ.

We can notice that the FID and the second order echo ($t = 2\tau$) spectra present narrower and more symmetrical lines than the first ($t = \tau$) and third ($t = 3\tau$) echoes. It is possible to discern a quintuplet structure for the FID, the first echo, and the second echo spectra, while the third echo had a triplet-like structure. The mean line widths around the 48.9 MHz peak were 100, 250, 60, and 200 kHz, for the FID, the first, the second, and the third echo spectra, respectively. Owing to the broad lines of the first and the third echoes, their mean line widths were estimated by dividing the half-width at half-maximum by the number of lines in the multiplet structure. These results are summarized in Table 2. The alternating behavior of the

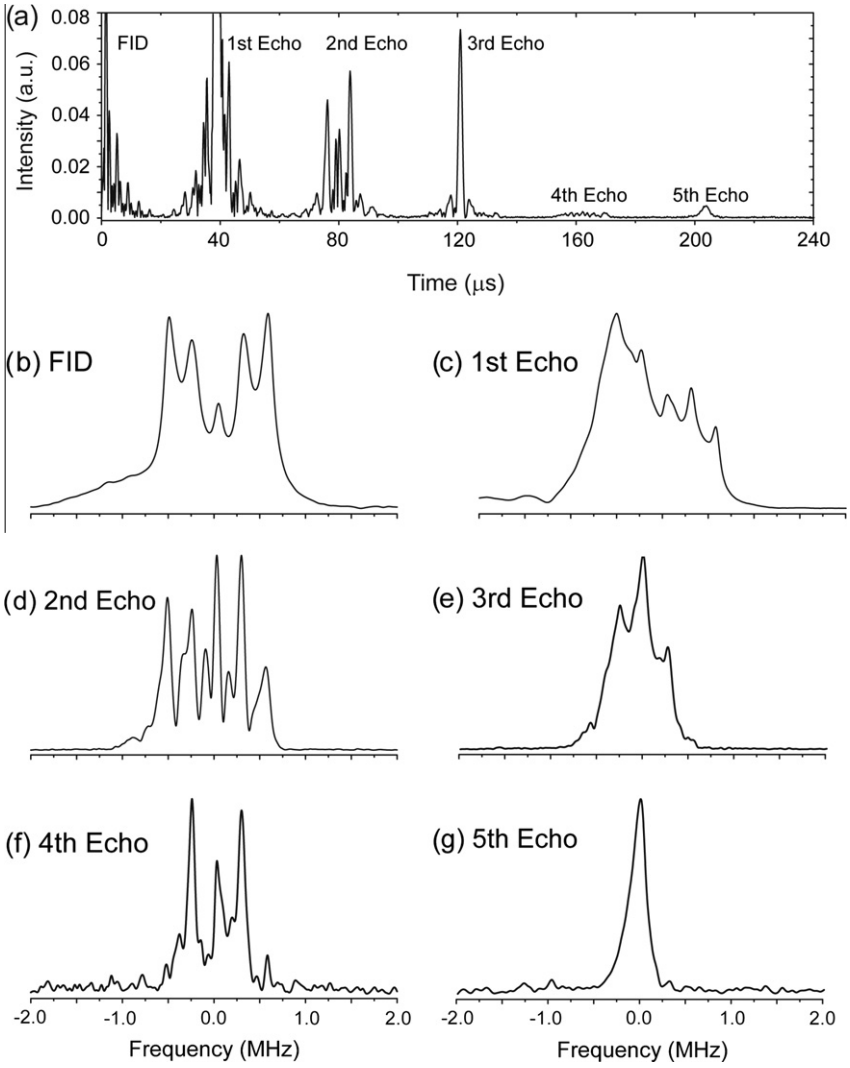

Fig. 5. ^{27}Al NMR time-domain signal (a) and the Fourier transform of each part (b–g), obtained with the two-pulse sequence (Fig. 1) applied at the single carrier frequency of 48.9 MHz. For convenience, the amplitudes of the FID and first echo (normalized to 1) have been reduced in scale, to allow the remaining echoes to be seen.

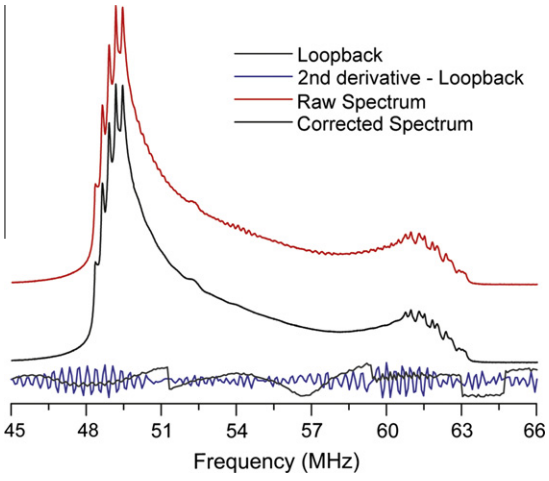

Fig. 6. Raw ^{27}Al NMR spectrum obtained from the first echo ($t = \tau$) together with the loop-back curve, its second derivative, and the corrected spectrum. The spectra were obtained by frequency sweep and processed by the FT method.

line widths shown in Table 2 can be qualitatively appreciated in the six spectra of Fig. 5b–g, where we can see a clear distinction between the even and odd echo orders. Odd echoes show line widths substantially broader than the even ones and the FID.

5. Discussion

The characteristics of the Gd spectra are in agreement with the theory discussed in Section 3 regarding the spectral line widths. The data obtained show that the Gd nuclei experience the complete inhomogeneity condition. This evidence is drawn from the spectral widths of the central and satellite transitions (Figs. 2a), where both interactions, Zeeman and quadrupolar, are much broader than the inverse of the echo time. The complete inhomogeneity assumption is further reinforced by the absence of the second-order echo and of the satellites in the third order echo, in Fig. 2. The absence of harmonic components in the quadrupolar oscillation experiment is also indicative that the quadrupolar interaction dispersion is very large for the Gd nuclei.

The discussion of the Al data is a little more involved. The main result is the enhanced spectral resolution of the even echoes compared to the odd ones (Figs. 5 and 7, and Table 2), especially over

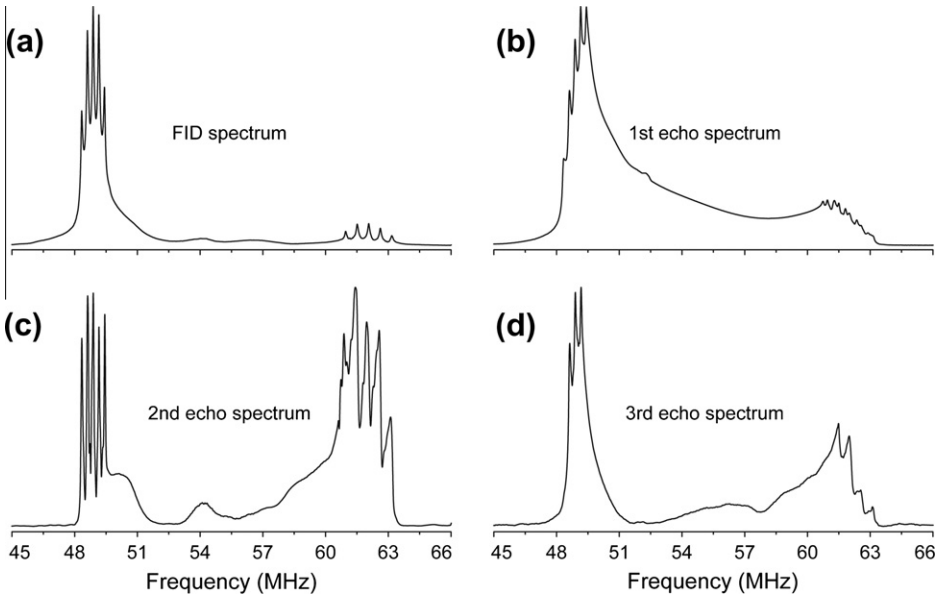

Fig. 7. ^{27}Al NMR spectra obtained from the FID (a) and the first three echoes, centered at $t = \tau$ (b), 2τ (c), and 3τ (d), generated with the two-pulse sequence of Fig. 1. The spectra were obtained with pulse frequency sweep and processed by the FT method.

Table 2
Estimated half-widths at half-maximum of the ^{27}Al spectral lines of Fig. 3 (single pulse) and Fig. 7 (two pulses). Peaks α and β correspond to the frequencies of 48.9 and 62.1 MHz, respectively.

Peak	Single pulse		Two pulses
	α (kHz)	β (kHz)	α (kHz)
FID	80	100	100
Echo 1			250
Echo 2			60
Echo 3			200

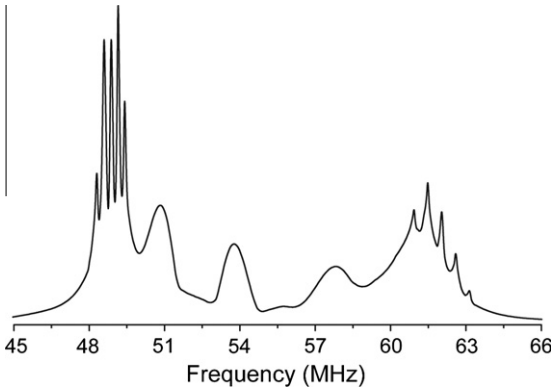

Fig. 8. First echo spectrum processed without the "negative" and central parts of the first echo time signal (removing the first points corresponding to 5.8 μs). The spectrum was obtained with pulse frequency sweep and processing the signals by the FT method.

the first order echo, which is used to study magnetic materials. The origin of such a distinction between the echoes of different order parity can also be explained in the light of the inhomogeneity conditions described in Section 3. Moreover, in a magnetic material like powdered $GdAl_2$, differing magnetic homogeneities are expected through the sample, arising from factors such as domains, domain walls, RF enhancement factor, etc. Therefore, let us analyze which inhomogeneity conditions could explain the differences in the spectral resolution of the echoes.

Since a complete inhomogeneity produces only odd order echoes, this condition should be the main cause of the large line widths of the odd echoes. Another indication is the number of spectral lines, where we can identify one, three, and five spectral lines for the fifth, third, and first order echoes, respectively, as expected for the complete inhomogeneity case.

From Table 1, we see that the only inhomogeneity case that produces all the even order echoes, as well as the odd ones, is the Zeeman case. As expected for this case, the spectra in Figs. 5 and 7 show that the even echoes show all five spectral lines with roughly the same line widths. There is not enough resolution to evaluate the Zeeman inhomogeneity contribution to the odd echoes, since it is superimposed on the broader signal from the complete inhomogeneity region.

There is no evidence for the existence of the quadrupolar inhomogeneity case, since there is no observable echo formation at half-integer intervals of τ.

Therefore, Tables 1 and 2 provide an estimate for the inhomogeneous broadening due to two regions of the sample: a more homogeneous one, with Zeeman dispersion from 60 to 100 kHz, and a less homogeneous one with Zeeman plus quadrupolar dispersion from 200 to 250 kHz. Since the echo time τ used in the experiment of Fig. 5 was 40 μs, we can infer that the quadrupolar dispersion in the Zeeman inhomogeneity region is much less than $1/\tau \sim 4$ kHz, while it is much greater than 4 kHz in the complete inhomogeneity region.

The relatively narrow line widths of the FID in Figs. 4 and 5 must be explained. From the discussion at the end of Section 3.3, the FID spectrum is expected to present broad line widths, $\Delta\omega_0 + \Delta\omega_q|m_k + 1/2|$, due to the complete inhomogeneity region. The observed narrow lines can be explained by the dead time before acquisition ($\Delta t \approx 2$ μs). Therefore, spectral components broader than $1/2\pi\Delta t \sim 80$ kHz are filtered out from the FID.

Inspired by the dead-time filtering effect on the FID signal and aware, from the discussion above, that the first order echo has a better resolution contribution we filtered the first echo too. This was done by applying a rectangular time window function to suppress the "negative" and central parts of the first order echo (removing the first points corresponding to 5.8 μs). The result is shown in Fig. 8. If we compare this spectrum with those shown

Table 3
Comparison between NMR frequencies calculated and measured by Bauer and Dormann [9], ν_{calc} and ν_1, respectively, and the frequencies ν_2 observed directly from Fig. 8.

$[hkl]$	ν_{calc} (MHz)	ν_1 (MHz)	ν_2 (MHz)
$[001]_{abcd}$	53.6	53.7	53.8
$[111]_{a}$	62.3	61.8	62.1
$[111]_{bcd}$	50.3	50.3	50.8
$[110]_{ab}$	58.1	58.0	57.6
$[110]_{cd}$	48.6	48.6	48.9

in Fig. 6 or Fig. 7b, we note a better resolution and the appearance of other peaks beyond the 48.9 and 62.1 MHz ones, which could also be observed with slight difficulty in Fig. 7c. To our knowledge, those peaks have not yet been reported, although they are expected from single crystal data [9]. Table 3 compares the expected Al peaks reported by Bauer et al. [9] and the ones obtained from the spectrum of Fig. 8 and shows close agreement for all peaks.

6. Conclusions

High-resolution zero-field NMR spectra were obtained for powdered $GdAl_2$ in the ferromagnetically ordered state at 4.2 K. The magnetization was measured after the application of single and two-pulse sequences. Both Gd and Al nuclei produced FID signals, showing that the field distributions in the test specimen were relatively narrow (transverse relaxation time for the FID greater than 2 μs). Multiple echo formation was observed for both nuclei when the two-pulse sequence was used. The origin of such echoes is the creation of multiple quantum states due to quadrupolar interaction, which evolve under both Zeeman and quadrupolar interaction dispersions, and are refocused by the RF pulse. A remarkable result was that the even echoes exhibited a substantially higher resolution than the odd ones (line widths ≈75% narrower for the ^{27}Al nuclei). We propose an explanation for such an effect as being due to signals originating from two regions in the sample with different inhomogeneity properties. According to this hypothesis, a more homogeneous region, with Zeeman dispersion from 60 to 100 kHz, produces all five echoes observed for the ^{27}Al nucleus, while a less homogeneous one, with Zeeman plus quadrupolar dispersion from 200 to 250 kHz, produces only the odd echoes among the five observed. In order to get information from the more homogeneous region contained in the first echo signal, we applied a rectangular time window to the echo center. As a result, we found new resonances between the 48.9 and 62.1 MHz peaks that had not yet been reported, but were expected from single crystal data [9]. Additionally, we applied the quadrupolar oscillation method to obtain the quadrupolar couplings of the ^{27}Al nucleus for the first three multi-quantum echoes. All three echoes showed oscillations at the expected frequencies, given that they are produced by MQ states. The results reported here indicate that other materials that present multi-quantum echoes could also benefit from spectral analysis of the even echoes, since the complexity of the distribution of interactions inside the magnetic material can produce a great variety of inhomogeneity conditions.

Acknowledgments

The Brazilian Science Foundations FAPESP, CNPq, and CAPES supported this work.

References

[1] J. Degani, N. Kaplan, Transferred magnetically induced Al-27 quadrupole interaction in $GdAl_2$, Phys. Rev. B 7 (1973) 2132–2135.
[2] N. Kaplan, E. Dormann, K.H.J. Buschow, D. Lebenbau, Magnetic-anisotropy and conduction-electron exchange polarization in ferromagnetic (rare-earth)Al_2 compounds, Phys. Rev. B 7 (1973) 40–49.
[3] D. Fekete, A. Grayevskey, N. Kaplan, E. Walker, NMR in single-crystal metallic ferromagnets – $GdAl_2$, Solid State Commun. 17 (1975) 573–576.
[4] E. Dormann, Nuclear spins as probes for magnetic coupling and crystallographic order in ferromagnetic intermetallic compounds, J. Magn. Magn. Mater. 6 (1977) 87–91.
[5] G.J. Bowden, J.M. Cadogan, W.M. Fairbairn, D.A. Griffin, A pulsed NMR-study of the rare-earth intermetallic compound $GdAl_2$, J. Phys. F – Met. Phys. 13 (1983) 191–205.
[6] E. Dormann, U. Dressel, H. Kropp, K.H.J. Buschow, Quadrupolar interaction of gadolinium nuclei at the cubic sites of ferromagnetic $GdAl_2$, J. Magn. Magn. Mater. 45 (1984) 207–218.
[7] T. Dumelow, P.C. Riedi, J.S. Abell, O. Prakash, Quadrupole interactions at the Al-27 nuclei of $GdAl_2$ as a function of pressure, temperature, holmium substitution and the application of an external-field, J. Phys. F – Met. Phys. 18 (1988) 307–322.
[8] I.S. Oliveira, A.P. Guimaraes, Power dependence of NMR in $GdAl_2$, Hyperfine Interact. 51 (1989) 959.
[9] M. Bauer, E. Dormann, Origin of zero-field Al-27 NMR-spectra of ferromagnetically ordered $GdAl_2$, Phys. Lett. A 146 (1990) 55–59.
[10] G.F. Zhou, H. Bakker, Spin-glass behavior of mechanically milled crystalline $GdAl_2$, Phys. Rev. Lett. 73 (1994) 344–347.
[11] M.A. Morales, D.S. Williams, P.M. Shand, C. Stark, T.M. Pekarek, L.P. Yue, V. Petkov, D.L. Leslie-Pelecky, Disorder-induced depression of the Curie temperature in mechanically milled $GdAl_2$, Phys. Rev. B 70 (18) (2004) 4407.
[12] P.M. Shand, C.C. Stark, D. Williams, M.A. Morales, T.M. Pekarek, D.L. Leslie-Pelecky, Spin glass or random anisotropy? The origin of magnetically glassy behavior in nanostructured $GdAl_2$, J. Appl. Phys. 97 (10) (2005) 1505.
[13] H. Abe, H. Yasuoka, A. Hirai, Spin echo modulation caused by quadrupole interaction and multiple spin echoes, J. Phys. Soc. Jpn. 21 (1966) 77–88.
[14] E.L. Hahn, Spin echoes, Phys. Rev. 80 (1950) 580–594.
[15] I. Solomon, Multiple echoes in solids, Phys. Rev. 110 (1958) 61–65.
[16] M.W. Dowley, Magnetic and quadrupolar echoes in aluminium metal, Solid State Commun. 3 (1965) 351–354.
[17] J. Butterworth, Spin echoes in solids, Proc. Phys. Soc. London 86 (1965) 297–304.
[18] G.N. Abelyashev, V.N. Berzhanskij, N.A. Sergeev, Y.V. Fedotov, Multiquantum effects and NMR in magnetically ordered substances, Phys. Lett. A 133 (1988) 263–265.
[19] V.O. Golub, V.V. Kotov, Y.A. Podyelets, A.N. Pogorely, Nuclear spin echo in magnetics with inhomogeneous hyperfine and quadrupole interaction, Hyperfine Interact. 59 (1990) 293–296.
[20] P.P. Man, E. Duprey, J. Fraissard, P. Tougne, J.B. Despinose, Spin-5/2 Hahn echoes in solids, Solid State Nucl. Magn. Reson. 5 (1995) 181–188.
[21] Y. Dumazy, J.P. Amoureux, C. Fernandez, Theoretical and experimental study of quadrupolar echoes in solid state NMR, Mol. Phys. 90 (1997) 959–970.
[22] J.C.C. Chan, Spin echoes in half-integer quadrupole systems, Concepts Magn. Reson. 11 (1999) 363–377.
[23] S.N. Polulyakh, N.A. Sergeev, A.A. Shemyakov, Spectra of multiquantum echo signals from quadrupole nuclei with half-integral spin in magnetically ordered materials, Phys. Solid State 42 (2000) 1675–1679.
[24] V.N. Berzhanskii, S.V. Kapel'nitskii, V.S. Pokatilov, S.N. Polulyakh, Multiple structure of two-pulse nuclear spin echo in cobalt films, Phys. Solid State 44 (2002) 88–91.
[25] A.M. Akhalkatsi, T.A. Gavasheli, T.O. Gegechkori, G.I. Mamniashvili, Z.G. Shermadini, W.G. Clark, Multiple NMR spin echoes in magnets: the echo structure and potential applications, J. Appl. Phys. 105 (7) (2009) D303.
[26] T.B. Massalski, Binary alloy phase diagram, Ohio, USA, 1992.
[27] J.S. Lord, P.C. Riedi, A swept frequency pulsed magnetic-resonance spectrometer with particular application to NMR of ferromagnetic materials, Meas. Sci. Technol. 6 (1995) 149–155.
[28] W.G. Clark, Pulsed nuclear resonance apparatus, Rev. Sci. Instrum. 35 (1964) 316–333.
[29] T.J. Bastow, Materials characterization by nuclear–quadrupole interaction, Z. Naturforsch. A – J. Phys. Sci. 49 (1994) 320–328.
[30] S.M. Dubiel, J.R. Tozoni, J. Cieslak, D.C. Braz, E.L.G. Vidoto, T.J. Bonagamba, Sublattice magnetism in sigma-phase $Fe_{(100-x)}V_x$ (x = 34.4, 39.9, and 47.9) studied via zero-field ^{51}V NMR, Phys. Rev. B 81 (18) (2010) 4407.